

A Hybrid Orographic plus Statistical Model for Downscaling Daily Precipitation in Northern California

GANESH R. PANDEY

California Department of Water Resources, Sacramento, California

DANIEL R. CAYAN

*Climate Research Division, Scripps Institution of Oceanography, University of California, San Diego, and
U.S. Geological Survey, La Jolla, California*

MICHAEL D. DETTINGER

U.S. Geological Survey, La Jolla, California

KONSTANTINE P. GEORGAKAKOS

*Climate Research Division, Scripps Institution of Oceanography, University of California, San Diego, La Jolla, and
Hydrologic Research Center, San Diego, California*

(Manuscript received 8 June 1999, in final form 5 July 2000)

ABSTRACT

A hybrid (physical–statistical) scheme is developed to resolve the finescale distribution of daily precipitation over complex terrain. The scheme generates precipitation by combining information from the upper-air conditions and from sparsely distributed station measurements; thus, it proceeds in two steps. First, an initial estimate of the precipitation is made using a simplified orographic precipitation model. It is a steady-state, multilayer, and two-dimensional model following the concepts of Rhea. The model is driven by the $2.5^\circ \times 2.5^\circ$ gridded National Oceanic and Atmospheric Administration–National Centers for Environmental Prediction upper-air profiles, and its parameters are tuned using the observed precipitation structure of the region. Precipitation is generated assuming a forced lifting of the air parcels as they cross the mountain barrier following a straight trajectory. Second, the precipitation is adjusted using errors between derived precipitation and observations from nearby sites. The study area covers the northern half of California, including coastal mountains, central valley, and the Sierra Nevada. The model is run for a 5-km rendition of terrain for days of January–March over the period of 1988–95. A jackknife analysis demonstrates the validity of the approach. The spatial and temporal distributions of the simulated precipitation field agree well with the observed precipitation. Further, a mapping of model performance indices (correlation coefficients, model bias, root-mean-square error, and threat scores) from an array of stations from the region indicates that the model performs satisfactorily in resolving daily precipitation at 5-km resolution.

1. Introduction

Observations of precipitation in mountainous regions are vital for forecasting total water yield and floods. In California, the major water-bearing region is the Sierra Nevada, but it contains only a sparse network of precipitation gauging stations. In particular, of more than 1100 National Oceanic and Atmospheric Administration (NOAA) cooperative and first-order stations within Cal-

ifornia, only 34 stations are located at elevations above 2000 m. Such sparse stations over rapidly varying terrain of this mountainous region are often unrepresentative of the overall precipitation patterns and are inadequate to represent the finescale details of precipitation. The spatial resolution of regional atmospheric circulation models (RCMs) is rarely less than 20–50 km. Even an operational model such as the Eta Model (Rogers et al. 1996) is not fine enough to capture the orographic details. Because small-scale cloud physics is not yet well understood (Rangno and Hobbs 1994), merely increasing spatial resolution does not mean more accurate estimates of precipitation (Colle et al. 1999). In addition, the computational demands of RCMs pro-

Corresponding author address: Ganesh Pandey, Dept. of Water Resources, Delta Modeling Section, 1416 Ninth St., Room 215-15, Sacramento, CA 95481.
E-mail: gpandey@water.ca.gov

hibit production of the long histories required for climate verifications.

To help to overcome these limitations, parameterized models have been developed to estimate finer-scale precipitation in mountainous regions. Previous studies, such as Rhea (1978), Sinclair (1994), and Hay and McCabe (1998) demonstrate that useful estimates of precipitation in mountainous regions can be made using approximate parameterizations of orographic mechanisms and cloud processes. However, the precipitation process in mountainous regions is a scale-dependent phenomenon (Robichaud and Austin 1988). Thus, the success of a simplified model in resolving finer-scale precipitation depends upon the mountain geometry (Brader and Roch 1978; Gocho 1978; Hill et al. 1981) and on the velocity and stability of air parcels flowing over the mountain (Collier 1975; Bell 1978; Hill et al. 1981; Dore and Choulaton 1992). Simplified models are generally suited to larger mountains, for higher wind velocities, and for near-neutral air profiles.

Northern California would seem to be an optimum location to implement such an orographic model because it lies directly downstream of an extratropical oceanic storm track whose events are primarily in winter and are not dominated by convection. Analyses of historical precipitation and sounding data show that most of the precipitation events in the Sierra Nevada are associated with moisture-laden southwesterly winds (Pandey et al. 1999). Along this southwesterly trajectory, most of the Sierra Nevada geometry could be classified as large mountains. Thus, a simple parameterized model may provide an attractive alternative to generate precipitation at finer scales in the data-sparse regions over northern California.

The purpose of this paper is to evaluate a methodology to resolve precipitation at finer scales in the mountainous region of the Sierra Nevada and in northern California. The method combines information from upper-air profiles and observed precipitation from gauging stations. First, to derive the precipitation distributions from the upper-air conditions, we implement a simplified two-dimensional orographic precipitation model following the concepts of Rhea (1978). The model is driven by National Centers for Environmental Prediction–National Center for Atmospheric Research (NCEP–NCAR; Kalnay et al. 1996) $2.5^\circ \times 2.5^\circ$ gridded reanalysis wind and humidity profile data to provide daily precipitation estimates at 5-km resolution. Second, the orographic model precipitation is then adjusted by minimizing errors between model precipitation and observed precipitation from nearby stations. This adjustment is intended to account for the detailed cloud processes not considered by the orographic model. Simulated precipitation is compared with observed station records that were not used in the model development to evaluate the model performance. The scheme generally replicates fluctuations and heavy extremes of the daily precipitation over the region.

2. Data and methodology

a. Input data

For most model runs and analyses herein, daily precipitation data from 170 cooperative National Weather Service observer and first-order precipitation stations located between 35° and 42°N in northern California were obtained from NOAA. Figure 1 shows the topography of the area along with the locations of the precipitation stations employed. The selection of stations was made to represent the northern half of California including coastal lowlands and coastal mountains, the central valley, and the Sierra Nevada. The bulk of this study uses data from the period 1986–95; for a limited set of validation runs 1980–85 data were also included. Also included during 1980–85 was a special set of precipitation data recorded during the Sierra Nevada cloud seeding experiment program.

Profiles of the upper air that consist of height, temperature, wind direction, wind speed, and relative humidity at “mandatory” levels (i.e., at 50-hPa intervals) from 900 to 300 hPa were taken from $2.5^\circ \times 2.5^\circ$ gridded NCEP–NCAR reanalysis fields (Kalnay et al. 1996). The gridded reanalysis data cover the area between 35° – 42.5°N and 117.5° – 125°W and are available on a daily basis.

The majority of precipitation events in California occur during winter, that is, approximately from December through April. Thus, the orographic model is tested for days during some of the core months of winter: January, February, and March (JFM). The distribution of the mean daily JFM precipitation is shown in Fig. 2. To calculate the mean daily precipitation, days having nonmissing records of precipitation, which include days with zero precipitation, were averaged for stations having at least one year on record. In general, stations located in the coastal mountains and on the west face (windward side) of the Sierra Nevada get more precipitation whereas stations in the central valley, on the east face (leeward side) of the Sierra Nevada, and in the northeastern part of California get less precipitation. This distribution of mean daily precipitation shows the orographic nature of the wintertime precipitation in California.

b. Orographic precipitation model

1) RHEA MODEL

Rhea (1978) developed a steady-state, multilayer, two-dimensional [alongwind and vertical (x, z)] orographic precipitation model for hydrological purposes. The model requires humidity, wind, and temperature soundings from nearby radiosondes as well as topography of the area (Fig. 3). In the beginning, the observed wind directions from six nearby stations were interpolated to the center of the study area. The study area was

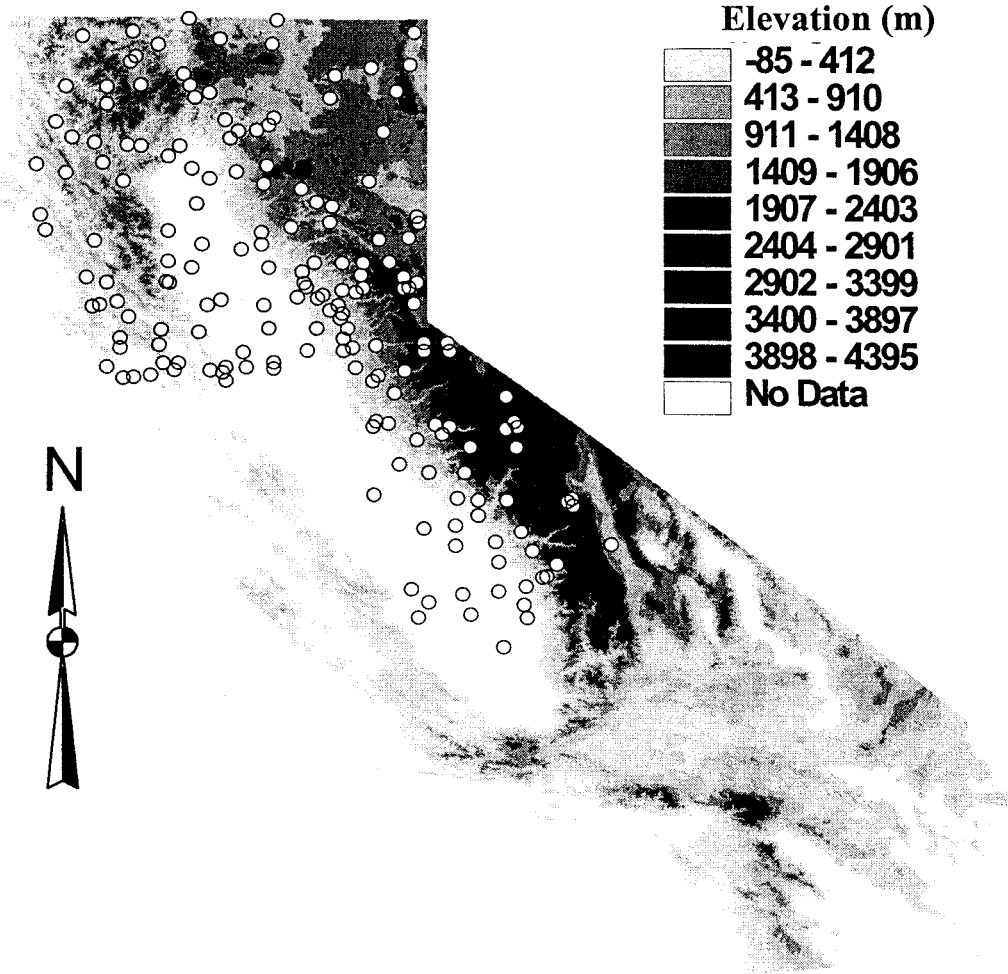


FIG. 1. Topography and the locations of the precipitation stations over the study area.

then rotated such that the y dimension was aligned parallel to the mean 70-kPa wind (to the nearest 10°). The profiles of upper-air soundings from six sites were interpolated to the upwind edge (i.e., along the x axis) of the study area. It was assumed that the horizontal flow of the air within the study area is along this y direction and its vertical displacement is proportional to the ground elevation profile. The temperature and humidity of each parcel of air passing through the study area were assumed to evolve by moist adiabatic condensation (or evaporation). Under these assumptions, the condensation rate would be proportional to the horizontal velocity and the humidity mixing ratio at the grid center as modified by an upward motion of air parcels. Rhea focused on upward air parcel motions induced by local variations of topography. The total condensation was multiplied by an “efficiency factor” to estimate the precipitation at ground level. Rhea’s efficiency factor, which parameterizes the cloud microphysical processes, was taken as a fraction of the cloud-top (defined as the highest layer having relative humidity greater than 65%) tem-

perature at the upwind edge of the study area. (In the version of the model employed here, a new form of the efficiency factor is used to account for upstream temperature gradient, moisture transport, and wind direction.) The estimated precipitation was interpolated to the unrotated grid centers using an inverse distance method. The model was tested for 5- and 10-km grid spacing using 12-h sounding data in Colorado. The performance of the model was validated using observed data from snowpack telemetry (SNOWTEL) stations and flows from the catchment. For most of the studied cases, the correlation between observed and model-derived precipitation was near 0.8. Hay (1996) and Hay and McCabe (1998) modified the Rhea model by incorporating Geographical Information System manipulations. Using hydrologic and topographic data from the Gunnison basin in Colorado, Hay also executed the Rhea model in a stochastic mode and implemented algorithms to find the optimal spatial scales, model parameters, grid rotation increment, and subdivision for the basin.

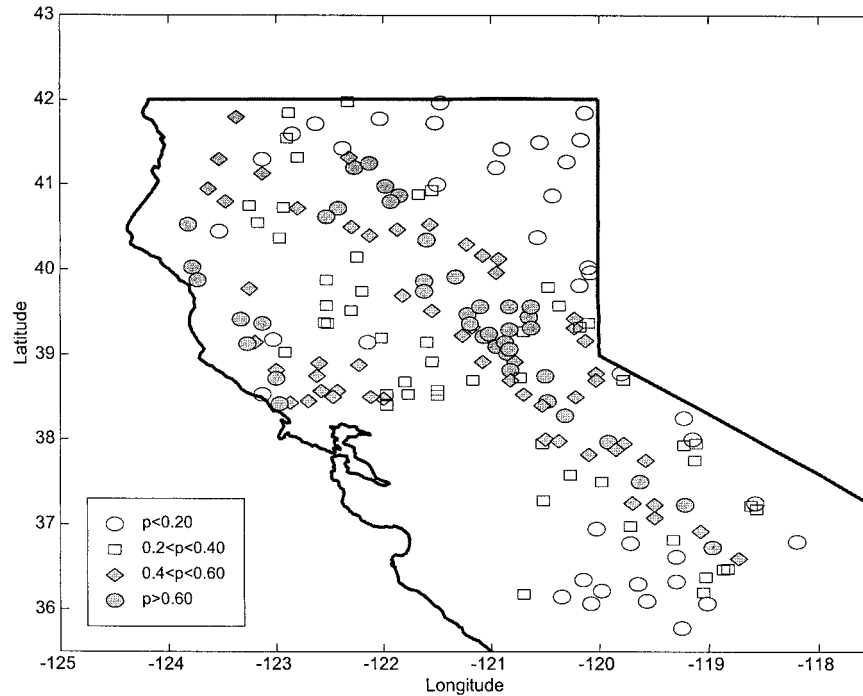


FIG. 2. Mean daily winter (Jan, Feb, and Mar) precipitation P (cm day^{-1}) for 1988–95 seasons for the Sierra Nevada and northern California.

2) OROGRAPHIC MODEL

The orographic precipitation model implemented here to generate the initial distributions of precipitation is a steady-state, multilayer, two-dimensional model following the concepts of Rhea (1978). Major refinements and alterations to the model and its parameters were instituted to yield results in better agreement with precipitation observations over the northern California domain. A schematic of the precipitation model is presented in Fig. 3. For any day, a profile of upper-air conditions is taken from the nearest reanalysis grid and is used to drive the model. The study area is divided into a fine “reference” grid, and the locations (longitude and latitude) of grid centers are determined. A grid of the same resolution is then rotated at its center such that one side of the rotated area is aligned along the x axis, the direction of the 700-hPa wind (to the nearest 10°) entering the study area. Both the upwind edge of the rotated area and the driving station are assumed to have the same atmospheric profiles. For the rotated area, ground elevations of the grid cells were extracted using the Digital Elevation Model and used with a spacing of 5 km. The air parcel blows from the upwind edge of the rotated area to its opposite side. It is assumed that, during its entire course, the parcel flows along a straight path. At any instance, the vertical position of the horizontally moving parcel (rise/fall) is determined by the profiles of the underlying topography. As a parcel rises, it cools, and, once the parcel cools to saturation with respect to water, further lifting generates precipitation.

At any height level l , total precipitation generated by orographic uplift along the grid interval $\Delta\alpha$ in the rotated grid is estimated by (Rhea 1978)

$$r_{i,l} = \frac{\Delta p_l v_l}{\rho_w g \Delta x} (E \Delta m_l), \quad (1)$$

in which $r_{i,l}$ is the precipitation rate between adjacent grid cells i and $i + 1$, Δp_l is the mean layer thickness in pressure units, v_l is the mean layer wind velocity, ρ_w is the density of water, g is acceleration caused by gravity, and E is a precipitation efficiency factor. The quantity Δm_l is the change in the total liquid water content and is equal to the total amount of condensation necessary to prevent supersaturation with respect to liquid water as the parcel moves up or down to cross topography plus any liquid water transported from the grid cell immediately upwind. After Rhea, E gives the fraction of the total condensate that falls as precipitation. The remaining condensate is transported to the next grid cell downwind. Note that Eq. (1) does not actually calculate the orographic uplift. However, as will be explained later, this effect is known in terms of Δm_l .

At each grid cell, calculation of the precipitation proceeds downward from the cloud-top level to the 900-hPa-level height. The cloud-top level is defined to be the highest layer having relative humidity greater than 65% and not underlaid by any layers having relative humidity below 25%. If any of the underlying layers has relative humidity less than 25%, the cloud-top level is further lowered to this level. If the relative humidities

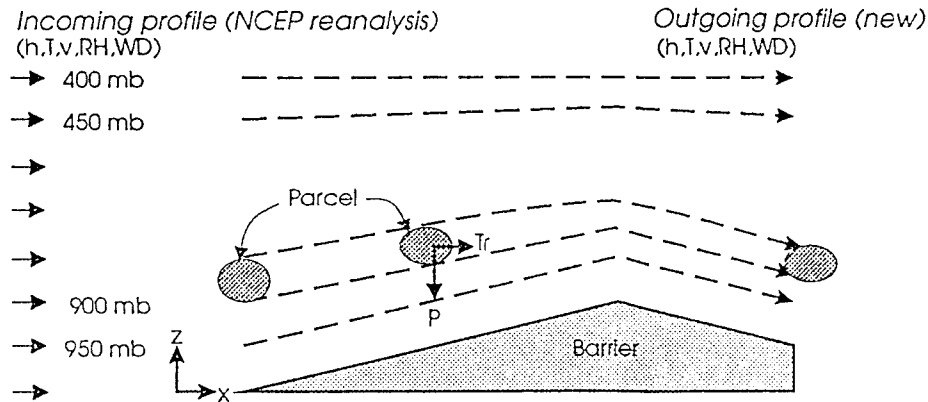
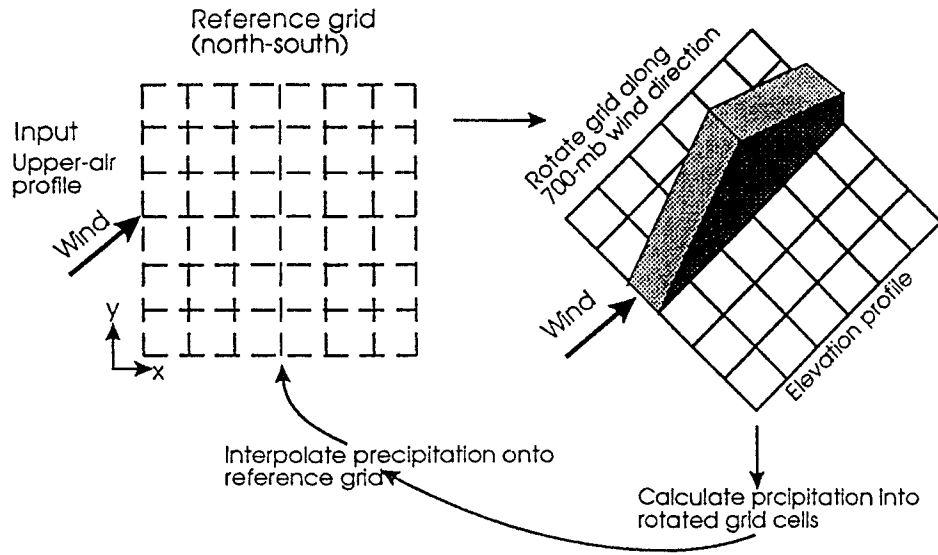


FIG. 3. Schematic of the Rhea orographic precipitation model (h = geopotential height, T = temperature, v = wind speed, RH = relative humidity, and WD = wind direction).

of all layers at the upwind edge are less than 25%, then precipitation in the entire region is set to zero. This definition of the cloud-top level and cutoff relative humidity were based upon empirical observations using historical sounding data from Oakland and precipitation from the Sierra Nevada. The total simulated precipitation P_i at the ground is obtained by integrating Eq. (1) from the lifting condensation level (LCL) to the cloud-top level (Ctop) as

$$P_i = \sum_{l=LCL}^{Ctop} r_{i,l} = \sum_{l=LCL}^{Ctop} \frac{\Delta p_l v_l}{\rho g \Delta x} (E \Delta m_l). \quad (2)$$

Using the precipitation given by Eq. (2) for rotated grid cells, precipitation at the i th reference grid cell is interpolated according to

$$P_{r,i} = \frac{1}{\sum 1/d_k} \sum_{k=1}^4 \frac{P_k}{d_k}, \quad (3)$$

in which $P_{r,i}$ is the interpolated precipitation for the reference grid, P_k is the total precipitation at the k th closest grid of the rotated area, and d_k is the distance between the i th reference grid cell and the k th closest cell of the rotated grid.

The model is driven in turn by at least three upper-air profiles. Assumption of a straight parcel trajectory precludes any possibilities of wind flowing along rather than across the mountain barrier. By driving the model with several separate upper-air profiles with their (usually) varying wind directions, errors caused by neglecting deviations of winds from straight-line paths across the topography are minimized. If wind directions of all

profiles are the same, then the lateral flow effects are not considered. However, each profile is expected to give different ground precipitation because of the variations in the temperature, humidity, and wind velocity of each profile. At each reference grid cell, the total value of the model-derived precipitation ($P_{s,i}$) is taken as the average of the precipitation obtained from N runs. That is,

$$P_{s,i} = \frac{1}{N} \sum_{k=1}^N P_{r,k}, \quad (4)$$

in which $P_{r,k}$ is the precipitation derived from the k th profile, and N is the total number of upper-air profiles used to drive the precipitation model.

3) TOTAL CONDENSATES

Between any two rotated grid points i and $i + l$, the change in the total condensate or total liquid water content (Δm_l) is the sum of two parts: that contributed by the local condensation due to uplift ($\Delta m_{l,C}$), and that contributed by the incoming air ($\Delta m_{l,T}$):

$$\Delta m_l = \Delta m_{l,C} + \Delta m_{l,T}. \quad (5)$$

The local condensation due to parcel uplift is given by

$$\Delta m_{l,C} = \frac{dq_s}{dh} \Delta h_l, \quad (6)$$

where Δh_l is the change in parcel elevation between grid points, and dq_s/dh is the rate of change in the saturation mixing ratio of water vapor with elevation. The change in parcel elevation between grid cells (Δh_l) is varied linearly with pressure; it varies from being equal to the change in ground elevation at 900 hPa to being 0 at 300-hPa pressure height. The change in the parcel elevation changes its temperature, and, depending upon the saturation condition at the upstream grid cell, the parcel temperature will follow either pseudoadiabatic or saturated-adiabatic lapse rate. This newly determined parcel temperature is used to calculate the rate of change in the saturation mixing ratio. Thus, the local condensation is a function of the profile of underlying topography and keeps on changing from one grid center to the other as the parcel passes through the rotated area.

The transported condensates to the next grid cell are connected to the total condensates via the efficiency factor as

$$\Delta m_{l,T,i+1} = (1 - E)(\Delta m_{l,i}). \quad (7)$$

The initial estimate of the transported condensates is made based upon the saturation condition of the atmospheric profiles. At the beginning, the rotated grid cell is augmented by adding an imaginary grid at its upwind edge. The elevation of the added grid is taken as 0.9 times the ground elevation at the upwind edge, and the local condensates are generated. If the entering

parcel is unsaturated, then the initial amount of condensates transported into the area is set equal to the negative of the saturation deficit, that is,

$$\Delta m_{l,T} = -\frac{dq_s}{dh} \delta h_l \quad (8)$$

in which δh_l is the elevation difference between LCL and parcel height. This negative ‘‘condensate’’ corresponds to the amount of uplift condensation that has to be developed by Eq. 6 before precipitation can begin along the parcel trajectory. Where topography and parcels are descending, evaporation of the falling condensates is assumed to proceed immediately, to keep the lowest layers saturated. At any layer, if all of the falling condensates are fully evaporated and still the parcel remains unsaturated, the negative of the saturation deficit is carried out to the downstream grids. Precipitation is constrained to occur only when Δm_l becomes positive.

In the precipitation model, then, the location of maximum precipitation is decided by the sequence of uplift, cooling, and transport. Thus it varies from day to day, depending on factors such as wind direction (Fig. 3) and other aspects of the atmospheric profile. This formulation is compatible with theoretical and empirical evidence on the locations of the maximum orographic precipitation, provided by Alpert (1986) and Daly and Johnson (1999, personal communication).

c. Model calibration

The precipitation model was calibrated by varying the precipitation efficiency to minimize the overall square error between observed and simulated daily precipitation at a group of stations located in the central Sierra Nevada within the training period (i.e., JFM of 1986 and 1987). The training period was chosen for the calibration of the model because it included a wide variety of storm events, from relatively small to historically large forms. The efficiency factor connects total condensation to orographic precipitation and represents—in a much simplified form—the cloud microphysical processes. Ideally, the processes represented by this factor should be dependent on gridcell size, mountain geometry, wind velocity, and microphysical properties of the clouds simulated (Rhea 1978).

There is high sensitivity of precipitation to the efficiency factor and thus the large and essentially irreducible uncertainty associated with it. Hay (1996) presented multiple model runs with a wide range of efficiency factors. In similar models by Speers and Mass (1986) and Speers-Hays (1991), the efficiency factor was taken as 0.5, which is the average of condensation-to-precipitation ratios that Elliot and Shafer (1962) calculated for the Santa Ynez and San Gabriel Mountains of coastal California. By considering the average ascending time of an air parcel moving at a constant velocity, Isakson (1996) varied the efficiency factor linearly from 0 at the coastline to a maximum of 0.4 at

the highest point over the Judean Mountains of Israel. Recently, for the Colorado regions, Gaudet and Cotton (1998) expressed the efficiency factor as a linear function of the temperature at the highest saturated level in the atmosphere.

In the current precipitation model, the efficiency factor is parameterized to account approximately for the influence of vertical temperature profile, stability conditions, and wind direction upon precipitation fallout (Pandey et al. 1998). That is,

$$E = \frac{k_1 k_2}{k_3}, \tag{9}$$

where k_1 , k_2 , and k_3 are empirical functions that depend on vertical temperature gradient, moisture transport, and orientation of the mountain barrier relative to the wind direction.

For precipitation events in the Sierra Nevada, both orographic lifting and availability of moisture play important roles (Pandey et al. 1999). Orographic lifting of air parcels is provided by the interaction of wind with the underlying terrain, and the amount of total moisture transport is decided by the temperature, velocity, and relative humidity of incoming wind. In historical profiles of the moisture transport from Oakland soundings, usually most of the moisture was concentrated at levels

below 700 hPa; at higher levels, cold temperatures limit moisture transport, and, at lower levels, reduced wind speeds restrict it. Thus, warm temperatures in the lower layers that carry most moisture and cool temperatures in the upper layers to condense the moisture are expected to be most favorable for orographic precipitation. Thus, function k_1 is defined as

$$k_1 = -0.01(T_{550} - T_{700}), \tag{10}$$

in which T_{550} and T_{700} are air temperatures, in degrees Celsius, at 550 and 700 hPa, respectively. The functional form used in Eq. (10) is very similar to the one used by Gaudet and Cotton (1998) to downscale precipitation in the Colorado region. The maximum temperature differences between these two layers occur when the lapse rate is near dry adiabatic; a temperature profile under this condition would also imply that conditions are favorable for dry convection (Gaudet and Cotton 1998). In contrast, when the air is fully saturated, then the temperature lapse rate (and thus $T_{550} - T_{700}$) is only one-half the dry adiabatic rate. Obviously, when the air is saturated there will be more moisture transport and hence a potential for higher precipitation.

The function k_2 accounts for the role of total incoming moisture and atmospheric stability conditions in augmenting orographic precipitation. It is expressed as

$$k_2 = \begin{cases} 1.00 & M \leq 1.15 \times 10^{-3} \\ (1 + M - 1.15 \times 10^{-3}) \times 0.25 \times 10^3 & 1.15 \times 10^{-3} < M \leq 2.15 \times 10^{-3} \\ 1.25 & M \geq 2.15 \times 10^{-3}, \end{cases} \tag{11}$$

where M is defined as

$$M = \frac{\theta_{e650} - \theta_{e750}}{h_{650} - h_{750}} \sum_{l=950}^{450 \text{ hPa}} w_l v_l, \tag{12}$$

where θ_{e650} and θ_{e750} are the equivalent potential temperatures; h_{650} and h_{750} are the heights in meters at the 650- and 750-hPa levels, respectively; w_l is the mixing ratio; and v_l is the mean wind speed in meters per second at each level. The first factor reflects the atmospheric stability conditions (Wallace and Hobbs 1977) and the second term is the total moisture transport. The amount of orographic lifting is dependent upon the direction of the wind in relation to the orientation of the range. The Sierra Nevada extends approximately northwest to southeast and presents maximum regional slopes to the southwest and northeast. Thus, winds blowing from the southwest and northeast experience maximum orographic lifting. However, winds from the north and east carry little moisture, and thus result in much less precipitation. Thus from the moisture transport and orographic

lifting, southwesterly winds are most favorable for precipitation in the Sierra Nevada. The function k_3 accounts for direction-dependent augmentation of moisture transport and parcel lifting over the Sierra Nevada. Its value varies between 1 and 3 with wind direction (θ_w) as given in Table 1.

Last, the value of efficiency factor E was constrained between 0 and 0.25, a limit also adopted by Gaudet and Cotton (1998). Thus, the functions k_1 , k_2 , and k_3 , and this limit of E , were determined by making a large number of runs to obtain the best agreement between simulated and observed precipitation for JFM 1986 and 1987. This parameterization was then fixed for the entire

TABLE 1. Variations in the values of k_3 with the wind direction.

Wind direction (θ_w)	Parameter (k_3)
$\theta_w < 170^\circ$	3
$170^\circ \leq \theta_w < 220^\circ$	$3 - [2/(220 - 170)(220 - \theta_w)]$
$220^\circ \leq \theta_w < 270^\circ$	1
$270^\circ \leq \theta_w < 340^\circ$	$1 + [2/(340 - 270)(\theta_w - 270)]$
$\theta_w \geq 340^\circ$	3

1988–95 simulation period. The values of functions k_1 , k_2 , k_3 , and E are determined based upon the conditions of the wind at the upstream edge of the rotated area and are not affected by changes in properties with transit. As described earlier, the same atmospheric profile is assumed to be valid throughout the upstream edge of the rotated study area. Thus, for a particular sounding profile used to drive the model, the magnitude of efficiency factor remains constant throughout the rotated area. However, if the model is driven by a different sounding profile, a new value of efficiency factor is expected. It is also noted that the local condensation given by Eq. (6) and hence the total condensation given by Eq. (1) is determined by the revised temperature and moisture conditions above the grid center. Thus, depending upon the sequence of uplift and cooling/warming of the parcel temperature, their values vary from grid to grid.

d. Model performance

The orographic model was run to generate the total daily precipitation over the Sierra Nevada range and in northern California. The validation period covered the winters (i.e., JFM) of 1988–95. The performance of the derived precipitation was evaluated using time series plots, correlation coefficient, model bias, root-mean-square error, and threat scores. The correlation coefficient is a measure of the linear dependency of the simulated precipitation with the observed. The bias gives an indication of the presence of systematic errors (under- or overprediction) in the model precipitation. It is defined as

$$b = \frac{1}{n} \sum_{i=1}^n (p_i^m - p_i^o), \quad (13)$$

in which b is the model bias; p_i^m and p_i^o are, respectively, the simulated and observed daily precipitation at a given site; and n is total number of days. Simulated precipitation was taken to be from the model grid point nearest the precipitation observation gauge being considered. The root-mean-square error (rmse) is closely related with the model-error variance and is a proxy of the reliability of the simulated precipitation. The rmse is calculated as

$$\text{rmse} = \sqrt{\frac{1}{n-1} \sum_{i=1}^n (p_i^m - p_i^o)^2}. \quad (14)$$

To account for large differences in precipitation at leeward and windward sides, the bias and rmse are normalized by each station's daily mean precipitation. Thus, their values are relative to the observed at-site mean. The threat score T_p is defined as (Giorgi et al. 1993)

$$T_p = \frac{N_c}{N_o - N_m - N_c}, \quad (15)$$

where N_o is the number of observed precipitation measurements in excess of threshold precipitation p , N_m is the number of simulations at or above the threshold, and N_c is the number of days on which both observed and forecast precipitation exceeds the threshold. The value of the threat score varies from 0 (completely unrelated) to 1 (for a perfect forecast) (Kuligowski and Barros 1998). Because of large differences in the precipitation amounts at the stations located on the east and west face of the Sierra Nevada, the threshold values were taken as relative to the mean station precipitation. Threshold values considered here were 0, 0.125, and 0.25 of the maximum precipitation at a given station.

Time series of the derived and observed precipitation at the Lake Spaulding, Donner Summit, Boca, Calistoga, and Ukiah precipitation stations for JFM of 1986 are plotted in Fig. 4. Lake Spaulding, Donner Summit, and Boca are located on the west side, near the ridge, and on the east side of the Sierra Nevada, respectively. Calistoga and Ukiah are coastal stations. Note that precipitation records from coastal stations, including the latter two stations, were not used to tune the model. During winter of 1986, the area was visited by two large storms, in the middle of February and early March, and also by three other smaller storms. The precipitation model captured individual storms and replicated observed daily precipitation. Generally, modeled precipitation was better for stations on the windward side of the Sierra Nevada and for stations in the coastal range of mountains. During the storm of mid-February, the model underestimated the precipitation peak for most of the stations located on the windward side (Fig. 4a). The model also predicted higher precipitation, such as in the beginning of the year, especially when the observed precipitation was small.

Average values of the correlation coefficients, model bias, root-mean-square errors, and threat scores of the derived daily precipitation are given in Table 2. In calculating the correlation coefficients, if both observed and simulated precipitation were zero, the day was excluded. This procedure was done to avoid the salutary influences on correlation when both the observed and simulated precipitation were zero. The orographic model produces estimated daily precipitation that typically correlates at around 50%. For lower-elevation range, the average value of the bias is less than 0.5 times the mean daily precipitation. As the station elevation increases, bias increases, and it is more than 2 times the mean daily precipitation for stations located in the highest-elevation range. For all elevation ranges, the values of the rmses are higher than 2 times the mean daily precipitation. Variations in the values of the threat scores also show that the performance of the orographic model deteriorates with elevations and threat values.

Distributions of the average correlation coefficients are shown in Fig. 5a. The correlation coefficients were higher (0.45) for stations located in the coastal areas and on the windward side of the Sierra Nevada than at

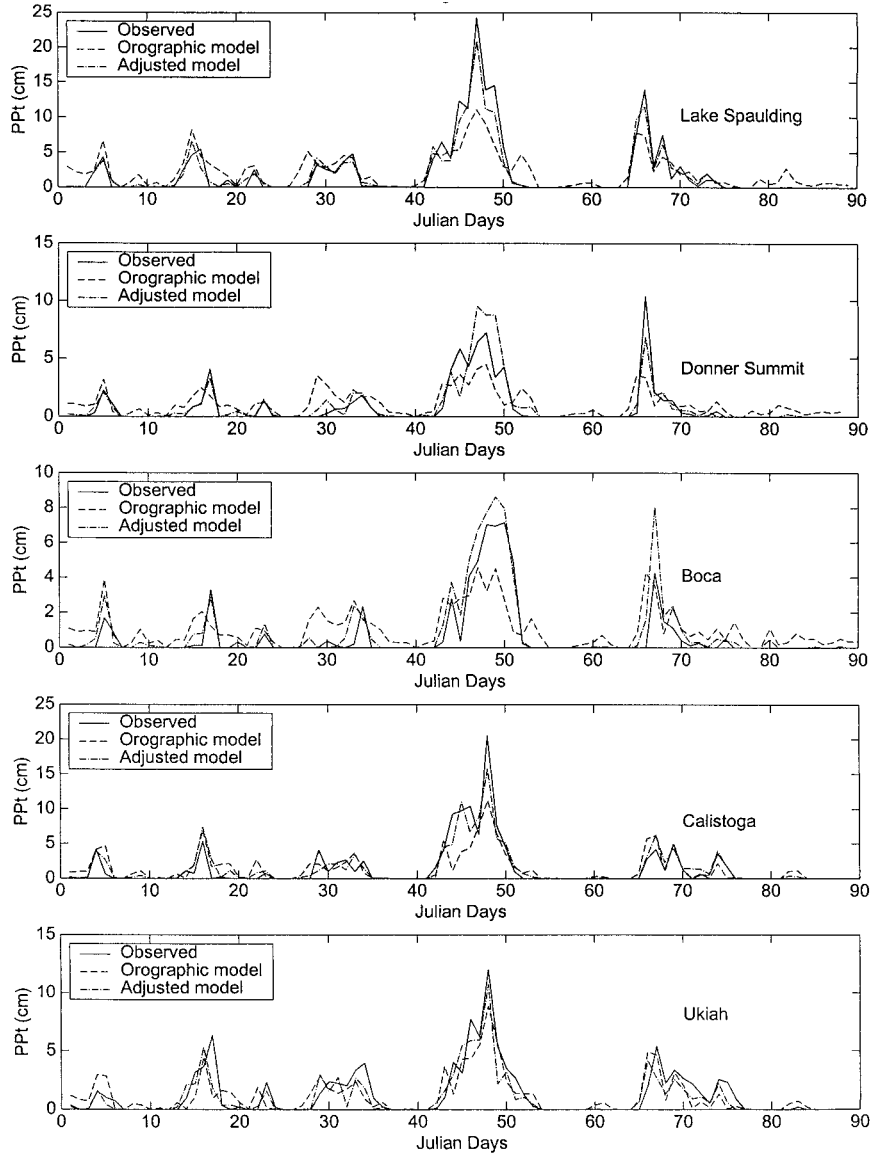


FIG. 4. Observed, orographic model-generated, and adjusted model-simulated daily precipitation (PP+) for Jan, Feb, and Mar of 1986 at representative precipitation stations.

TABLE 2. Average values of correlation coefficient (Corr.), bias, and rmse for simulated precipitation vs that observed at stations located at different elevation ranges. Mean ppt represents the mean daily precipitation for the period of JFM of 1988–95 and includes only nonmissing records. (Th1, Th2, and Th3 represent threat scores for threshold $p > 0$, $p > 0.125$ of at-site maximum precipitation, and $p > 0.25$ of at-site maximum precipitation, respectively).

Elevation (m)	Mean ppt (cm day ⁻¹)	Threat scores					
		Corr.	Bias	Rmse	Th1	Th2	Th3
<250	0.14	0.49	0.43	2.67	0.41	0.27	0.17
250–500	0.25	0.59	0.02	2.16	0.46	0.25	0.18
500–1000	0.21	0.51	0.40	2.36	0.43	0.31	0.20
1000–1500	0.17	0.48	1.59	3.75	0.37	0.28	0.19
1500–2000	0.14	0.44	2.17	4.47	0.32	0.24	0.17
>2000	0.16	0.52	2.14	3.91	0.36	0.25	0.23

those stations located on the leeward side. For stations located on the leeward side of the mountain barrier and central valley, the average values of the correlation coefficient were close to 0.3. This variation in the values of the correlation coefficient was very similar to the variations in the mean daily precipitation. Thus, the model performed well in areas that received higher precipitation.

Model biases are shown in Fig. 5b. Model biases range from less than 0.5 to more than 2 times the mean daily precipitation. It can be seen that simulated precipitation is less biased in coastal areas and on the windward side of the Sierra Nevada and is more biased for stations located in the central valley and on the lee side of the Sierra Nevada. Thus, in general agreement with

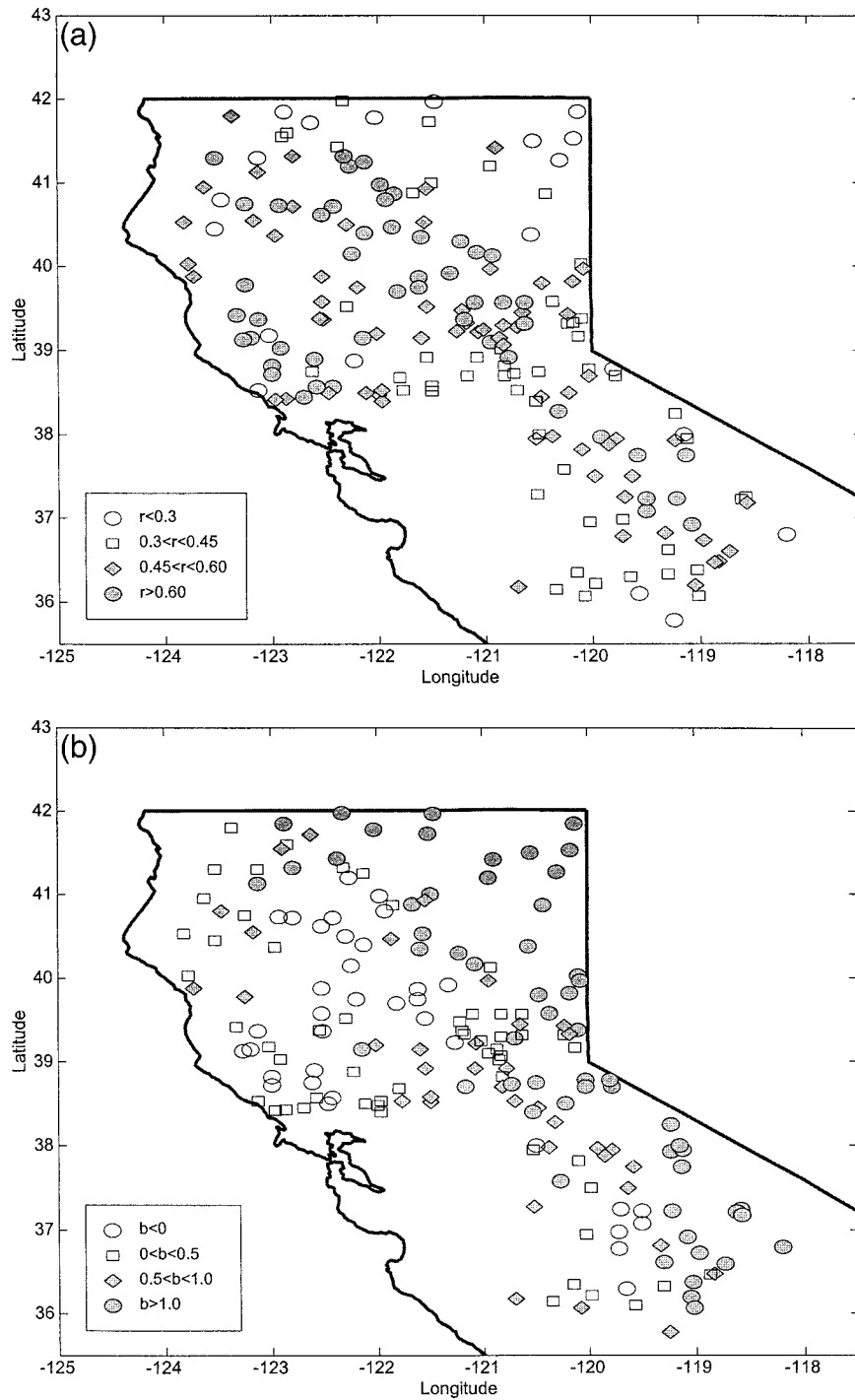


FIG. 5. (a) Correlation coefficient r between observed and orographic model-derived daily precipitation for stations located in the Sierra Nevada and northern California. (b) Standardized prediction bias b of the derived precipitation for northern California.

the distributions of the correlation coefficients (Fig. 5a), the performance of the model was inferior for leeward stations; it mostly overestimated precipitation.

The discrepancies between observed and simulated precipitation may be the combined outcome of the com-

parison method and model weaknesses. First, some discrepancies in the model performances could be attributed to the comparison method itself, such as point versus aerial output. The simulated precipitation at the reference grid cell nearest to a station is compared with

the observed precipitation totals. Thus, for a 5-km spacing, the location of station and grid point could be offset by as much as 3.5 km. Comparison between point versus aerial average will include inherent errors. In particular, this error could be a problem for stations located near the tops of the ridges, at which large variations between precipitation on the lee and wind sides develop over short distance.

Second, discrepancies between observed and simulated precipitation may also be attributed to limitations of the parameterization schemes of the orographic precipitation model. In the model, forced orographic lifting is the main mechanism that generates precipitation and there is no consideration of cloud microphysics. The convective precipitation component, which is parameterized through the modification of the efficiency factor, is weak. Assumptions of a constant velocity and straight parcel trajectory are other possible sources of errors.

In the region of complex terrain, recent studies by Colle et al. (1999) show that precipitation models such as the NCAR Fifth-Generation Mesoscale Model and the NCEP Eta-10 Model perform differently on the leeward and windward sides of the barrier; usually they tend to generate too much precipitation on the windward side and not enough precipitation on the leeward side. This result suggests that the precipitation process in orographic regions is still not well understood. Given the present state of understanding of the orographic precipitation process, increasing model resolution or adding more parameters does not necessarily imply more accurate forecasting of precipitation.

e. Adjustment of model precipitation using observations

In cases where the objective is to produce a more accurate mapping of precipitation than the orographic model alone or than simple interpolation of sparse precipitation observations, a hybrid approach may be useful. To this end, the model precipitation was adjusted using observed precipitation from nearby gauging stations such that errors in the model precipitation were minimized. At any gauging station, on each day, error between derived and observed precipitation (ϵ_r) was defined as

$$\epsilon_r = (p^m - p^o), \tag{16}$$

in which p^m and p^o are, respectively, the derived and observed precipitation. Equation (16) was used to determine the errors at grids in which gauging stations are present. For intermediate grids (i.e., at grid cells without gauging stations), errors in the derived precipitation were taken as the average of the errors from the four nearest gauging stations. That is,

$$\epsilon_f = \frac{1}{4} \sum_{i=1}^4 (p_i^m - p_i^o), \tag{17}$$

in which p_i^o is the observed precipitation at the i th near-

TABLE 3. Same as Table 2 but for the adjusted “simulated precipitation” from a jackknife procedure as judged against observed daily precipitation for JFM of 1988–95.

Elevation (m)	Mean ppt (cm day ⁻¹)			Threat scores			
	Corr.	Bias	Rmse	Th1	Th2	Th3	
<250	0.14	0.73	0.07	1.84	0.62	0.51	0.37
250–500	0.25	0.80	0.04	1.54	0.67	0.46	0.32
500–1000	0.21	0.76	0.10	1.65	0.63	0.49	0.39
1000–1500	0.17	0.66	0.35	2.51	0.56	0.40	0.32
1500–2000	0.14	0.63	0.38	2.75	0.49	0.47	0.37
>2000	0.16	0.71	0.35	2.05	0.57	0.44	0.35

est station from the considered grid cell, and p_i^m is the orographic model-derived precipitation at the considered grid cell. Equations (16) and (17) were used to determine the error field within the entire region. At any grid cell, to adjust the precipitation, this estimated error was subtracted from the precipitation derived from the orographic model. That is,

$$P_f = P_s - \epsilon_f, \tag{18}$$

in which P_s is the simulated precipitation from the orographic precipitation model and P_f is the error-adjusted precipitation. Note that the error field derived by using Eq. (17) uses information only from nearby gauging stations, whereas Eq. (18) is applied at each grid cell in the reference area. This adjustment procedure was then applied for each day in the 1988–95 period of JFMs. In the remaining sections, the adjusted model precipitation is also referred to as simulated precipitation.

f. Performance of adjusted model

The performance of the adjusted model precipitation was examined using a jackknife procedure. That is, for each day, the orographic model was run to obtain the initial distribution of precipitation. Then one gauging station was removed from the dataset. Using observed precipitation from the remaining stations, the model-generated precipitation was adjusted following the procedures described earlier. The adjusted precipitation was used to derive the daily precipitation for the site not included in the error adjustment. The steps were repeated by removing one station at a time. Thus the adopted jackknife procedure simulates ungauged site conditions.

Time series of the simulated and observed daily precipitation for representative gauging stations are shown in Fig. 4. The phase and the magnitude of the simulated precipitation resembles the phase and magnitude of observed precipitation. The adjusted model precipitation also reduced the excessive amounts of precipitation on the eastern side of the Sierra Nevada. Using the independent datasets, values of the correlation coefficient, model bias, rmse, and threat scores of the simulated daily precipitation are given in Table 3. Comparison of

Table 3 with Table 2 shows improvements in the performance of the simulated precipitation over precipitation derived through the orographic model. For example, average correlations increased from nearly 0.5 to nearly 0.7, and bias was reduced from nearly 3 times to less than 0.5 of the mean daily precipitation. For the heavy precipitation events, which occur in the midelevation range, average correlation between observed and resolved precipitation is about 80%. The rmse values varied between 1.5 to less than 3 times that of the mean daily precipitation. Improvements could also be seen in the values of the threat scores. For smaller threshold value, the threat score is about 0.6, and for higher threshold values it is in the range of 0.35. Table 3 also reveals that the simulated precipitation performed well in the lower-elevation (between 250 and 500 m) range, which also has higher average precipitation (about 0.25 cm day⁻¹).

Spatial distributions of correlation coefficient, model bias, and rmse are shown in Figs. 6a, 6b, and 6c, respectively. For most of the stations, the adjusted precipitations correlates at or above 50% or higher levels. The bias of the resolved precipitation is less than 0.5 of the mean daily precipitation, and rmse ranges from less than 0.5 to more than 2 times the mean daily precipitation. Comparisons of Fig. 6 with Fig. 5 shows significant improvements in the adjusted model performances for each elevation range and particularly for stations located in the leeward side of the Sierra Nevada.

Distributions the precipitation threat scores are shown in Figs. 7a–c. For a threshold value of $p > 0$, the threat score value is about 0.6. With an increase in the threshold value, the value of the threat score decreased. For a threshold value of 0.25 of the at-site maximum daily precipitation, the average value of the threat score is mostly higher than 0.3. The values of the threat scores are higher than typically given by most climate models (Olson et al. 1995). The decrease in the values of the threat scores with an increase in the precipitation threshold shows that the procedure is most effective in resolving the smaller events. Figures 6a–c show that resolved precipitation on the east side of the Sierra Nevada and central valley have smaller correlations, higher bias, and higher rmse values. However, aerial distributions of the threat scores (Figs. 7a–c) show that the adjusted model produces reasonable simulations of precipitation on both sides of the barrier. Even for the northeastern part of the domain, where the gauging stations are very sparse, the adjusted model performance is good.

Figure 8 shows the topography of the central Sierra Nevada region along with the locations of NOAA precipitation stations. Also shown are the locations of an independent set of 42 Sierra Nevada cloud seeding experiment precipitation stations that reported precipitation from 1980 to 1988. However, the data were not reported for each day. Thus, for the winter months, there were around 90 days of data available. Many of these Sierra Nevada cloud seeding experiment stations are

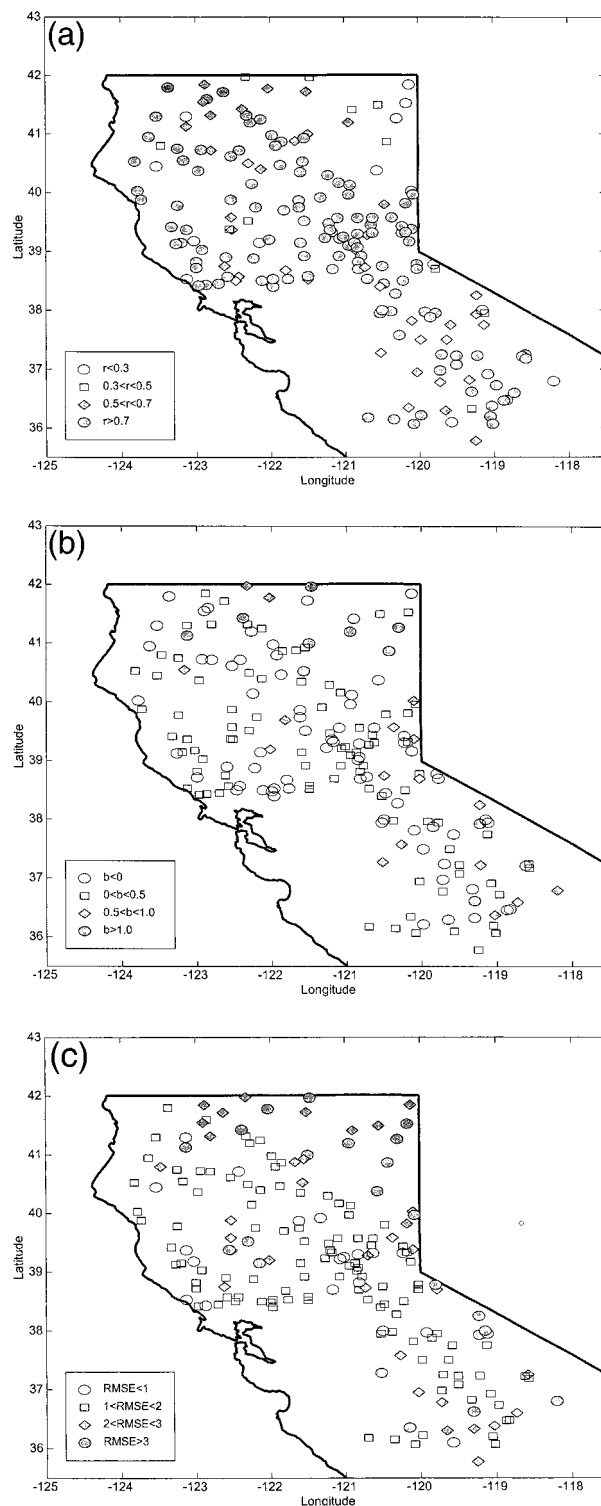


FIG. 6. (a) Same as Fig. 5a for adjusted orographic model precipitation. (b) Same as Fig. 5b for adjusted orographic model precipitation. (c) Standardized model rmse of the adjusted orographic model precipitation.

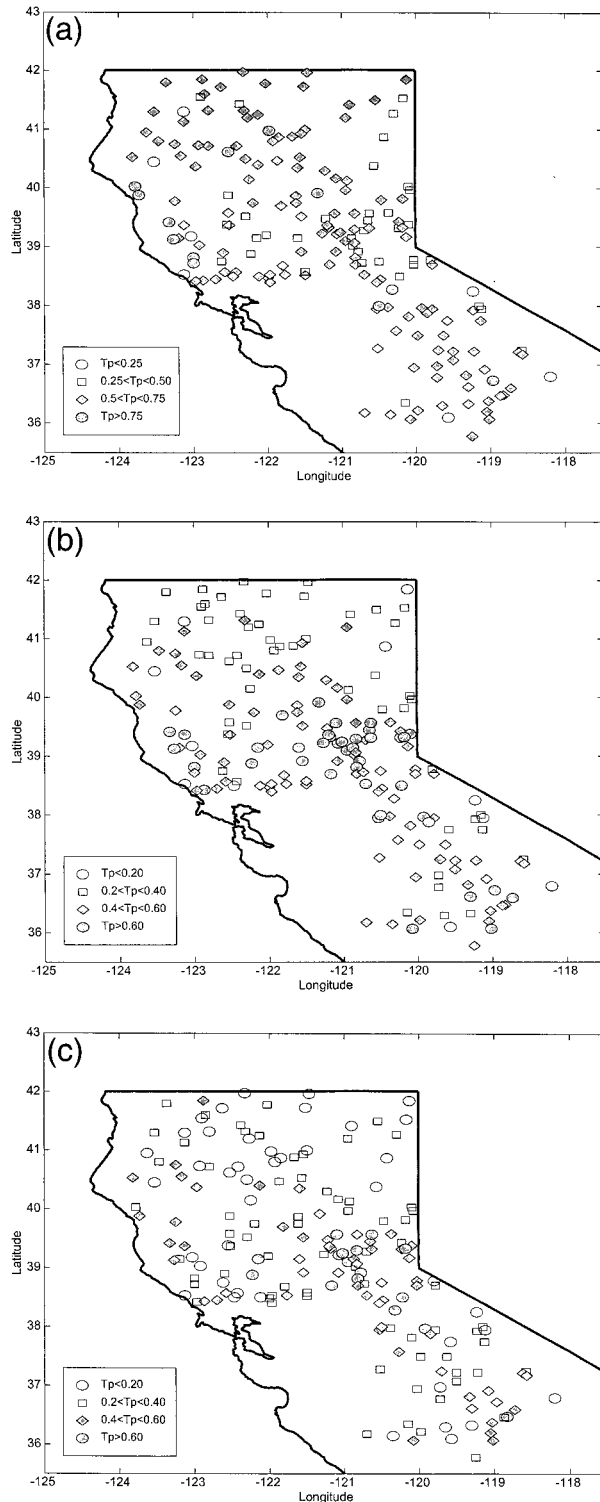


FIG. 7. (a) Threat scores T_p for adjusted orographic model precipitation for a threshold of nonzero precipitation (i.e., $p > 0$). (b) Same as (a) but for a threshold of 0.125 times the at-site maximum daily precipitation (i.e., $p > 0.125$ of at-site maximum daily precipitation). (c) Same as (a) but for a threshold of 0.25 of at-site maximum daily precipitation (i.e., $p > 0.25$ of at-site maximum daily precipitation).

located in areas with relatively dense gauging stations. Thus, this set of 42 stations was taken as an independent set of data for model validation.

At each Sierra Nevada experimental station, two sets of daily precipitation were derived. In the first case, daily precipitation was estimated using the simulated precipitation. The second set represents the precipitation derived from the nearest-neighbor method using the data from both cooperative stations and Sierra Nevada experimental sets. Thus available stations for the nearest-neighbor method form a very dense set of data. The precipitation derived from the nearest-neighbor scheme represents the weighted (by the inverse distance) average of the four nearest gauging stations. Again, to simulate an ungauged site condition, a jackknife procedure was used.

To examine the relative gains of using simulated precipitation over those obtained from the nearest-neighbor method, two linear models were developed. The first model expressed observed daily precipitation as a function of simulated precipitation. In the second case, observed daily precipitation was expressed as a function of precipitation derived from the nearest-neighbor method. A separate model was developed for each Sierra Nevada experimental station. Variations in the regression coefficient (R^2) from both models are shown in Fig. 9a. It can be seen that, at the majority of stations, the simulated precipitation outperformed the precipitation derived from the nearest-neighbor method. However, if the distance between two stations was small, then the nearest-neighbor method produced better estimates. Differences in the R^2 values from the two methods, shown in Fig. 9b, give the amount of additional variance explained by the simulated precipitation. Even for the dense network as shown in Fig. 8, the simulated precipitation explains an additional 5%–10% of the variance over the nearest-neighbor method.

3. Summary and discussion

A simplified approach has been described to estimate daily precipitation in the mountainous terrain of the Sierra Nevada and northern California. The scheme combines the precipitation generated from a simplified orographic precipitation model along with the sparse precipitation observations. The precipitation model, adopted from Rhea (1978), Hay (1996), and Hay and McCabe (1998), is a steady-state, multilayer, two-dimensional model. It is driven by the atmospheric profiles generated by atmospheric circulation model output and also requires the profiles of ground elevation along air trajectories. The model generates precipitation by assuming a forced vertical displacement of air parcels as they cross the mountain barrier along a straight trajectory. Condensation is assumed to arise by means of saturated ascent of air parcels. To account particularly for the lateral flow effects, the model is driven independently by at least three atmospheric profiles. The California

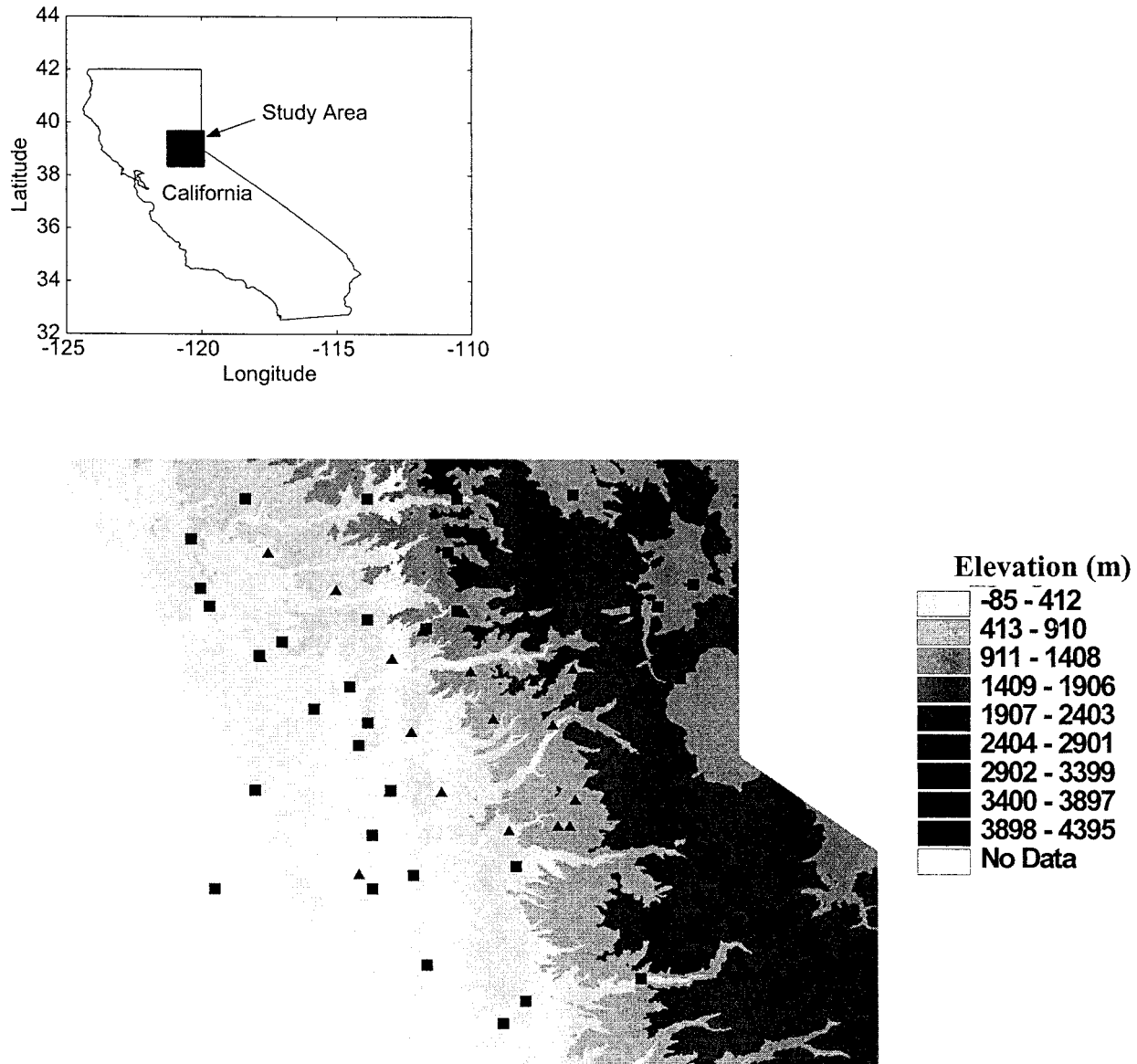


FIG. 8. Topography and location of the NOAA (square) and Sierra Nevada experiment (triangle) precipitation stations.

region is ideal for this scheme because it has severe relief and it lies directly downstream of the North Pacific winter storm track. The parameters of the model are tuned using the observed precipitation during the winters of 1986 and 1987. The performance of the model is verified using daily precipitation data from a network of 170 gauging stations from the Sierra Nevada and the coastal regions of California. The verification period covered the winters (January–March) of 1988 through 1995 and a special high-density dataset from 1980 to 1988.

For a 5-km spacing, the performance of the method in resolving precipitation was evaluated using a jack-knife procedure. The orographic model captured individual storm events; however, the leeside precipitation

was overpredicted. The orographic model produces estimated daily precipitation that typically correlates at 50% with observed precipitation using the independent validation dataset. For the heavy precipitation events, which occur near the foothills of mountain barriers, the correlation was nearly 60%. The orographic model precipitation was adjusted using the observations from gauging stations. The adjusted model precipitation reproduced well the maximum precipitation in the region. The excess precipitation given by the orographic model was reduced. The adjusted simulated precipitation performed better than the precipitation obtained from the nearest-neighbor method. Spatial distributions of the correlation coefficient, model bias, root-mean-square error, and threat score for the validation period show the

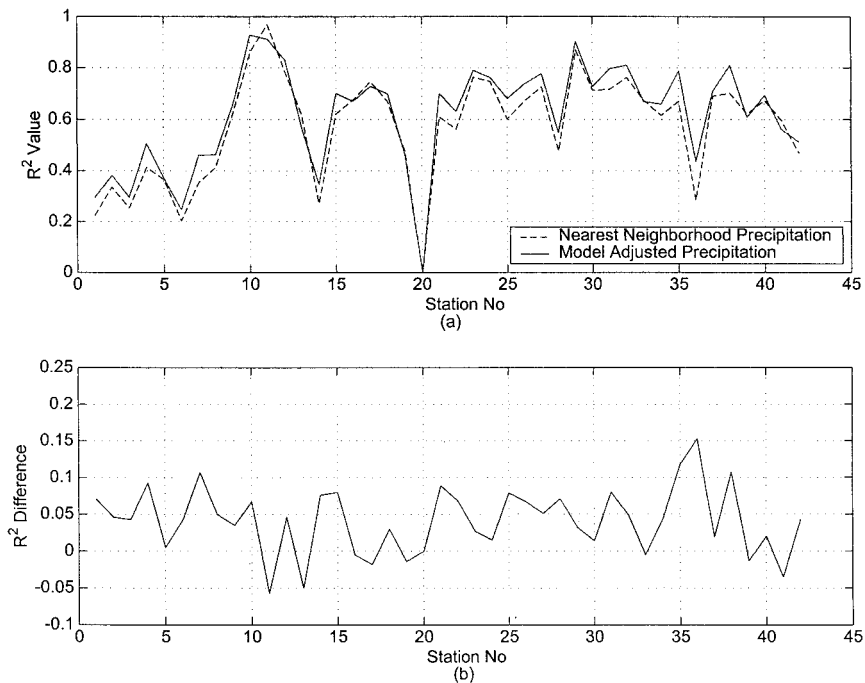


FIG. 9. (a) Regression coefficient (R^2) of the model expressing the observed Sierra Nevada experimental station daily precipitation as a function of derived precipitation. The stations are sorted according to station elevation, from lowest (station 1) to highest (station 42) (dotted line is R^2 of the model connecting observed precipitation with the precipitation derived from the nearest-neighbor method, and continuous line is R^2 of the model connecting observed precipitation as a function of the adjusted orographic-model precipitation). (b) Differences in the R^2 values of the two linear models expressing the observed Sierra Nevada experimental station daily precipitation as a function of derived precipitation. The first model expressed observed precipitation as a function of the precipitation derived from the nearest-neighbor method, and the second model expressed observed precipitation as a function of the simulated precipitation.

effectiveness of the schemes in resolving precipitation at finer scales. For all precipitation events, resolved precipitation correlates at around 60%, and for heavy precipitation events, the correlation was near 80%. For the coastal regions and stations located on the wind side of the Sierra Nevada, the bias in the simulated precipitation was less than 0.5 of the mean daily precipitation. Model threat scores were higher than those given by large-scale climate models. In general, as compared with the leeward side, the simulated precipitation is better on the windward side of the Sierra Nevada and over the coastal region.

The performance of the orographic model indicates that this approach could be used to complement daily precipitation observations in data-sparse regions over the entire study area. Another potential application of the scheme lies in downscaling forecasts or simulations provided by numerical circulation models to watershed scales. Specifically, output from global or regional circulation models could be used to drive the orographic precipitation model to resolve precipitation at finer scales. These resolved fields of precipitation could be used to drive hydrological-scale (e.g., 5–10 km) watershed models. Thus it will be possible to make appli-

cation forecasts (such as streamflow) using the output from circulation models, almost on a real-time basis. Retrospectively, using radiosonde profiles or wind and humidity from the NCEP–NCAR reanalysis profiles, it will be possible to generate the historical distributions of the precipitation over the region.

At present the model was used to simulate the wintertime (January–March) precipitation. Further work is needed to test it in simulating the precipitation for other seasons. This model can easily be used to produce temperature at each grid cell. Previous works by Rhea (1978) and Hay and McCabe (1999) have shown that this kind of orographic model can be applied to mountainous regions in Colorado, but studies are also needed to assess it for resolving finescale precipitation in other regions.

Acknowledgments. Funding was provided by the University of California Campus–Laboratory Collaboration (CLC) program by the NOAA Office of the Global Programs through the Experimental Climate Prediction Center and the California Applications Project and by NASA through the WP-ESIP Project. Cooperative and first-order station precipitation data were obtained from

the Western Regional Climate Center, courtesy of Dr. Kelly Redmond, and Sierra Nevada cloud seeding experiment station precipitation data were obtained from the Hydrologic Research Center. Discussions with Dr. Owen Rhea and Dr. Lauren Hay were very helpful, as were comments by three anonymous reviewers.

REFERENCES

- Alpert, P., 1986: Mesoscale indexing of the distribution of the orographic precipitation over high mountains. *J. Climate Appl. Meteor.*, **25**, 532–545.
- Bell, R. S., 1978: The forecasting of orographically enhanced rainfall accumulations using 10-level model data. *Meteor. Mag.*, **107**, 113–124.
- Brader, M. J., and W. T. Roach, 1977: Orographic rainfall in warm sectors of depressions. *Quart. J. Roy. Meteor. Soc.*, **103**, 269–280.
- Colle, B. A., K. J. Westrick, and C. F. Mass, 1999: Evaluation of MM5 and Eta-10 precipitation forecasts over the Pacific Northwest during the cool season. *Wea. Forecasting*, **14**, 137–154.
- Collier, C. G., 1975: A representation of effects of topography on surface rainfall within moving baroclinic disturbances. *Quart. J. Roy. Meteor. Soc.*, **101**, 407–422.
- Dore, A. J., and T. W. Choullarton, 1992: A three dimensional model of airflow and orographic rainfall enhancement. *Quart. J. Roy. Meteor. Soc.*, **118**, 1041–1056.
- Elliot, R. D., and R. W. Shafer, 1962: The development of a quantitative relationship between orographic precipitation and air-mass parameters for use in forecasting and cloud seeding evaluation. *J. Appl. Meteor.*, **1**, 218–228.
- Gaudet, B., and W. R. Cotton, 1998: Statistical characteristics of a real-time precipitation forecasting model. *Wea. Forecasting*, **13**, 966–982.
- Giorgi, F., G. T. Bates, and S. J. Nieman, 1993: The multiyear surface climatology of a regional atmospheric model over the western United States. *J. Climate*, **6**, 75–95.
- Gocho, Y., 1978: Numerical experiment of orographic heavy rainfall due to a stratiform cloud. *J. Meteor. Soc. Japan*, **56**, 405–422.
- Hay, L. E., 1996: Assessment of an orographic precipitation model in southwestern Colorado. Ph.D. thesis, University of Colorado, 127 pp. [Available from Department of Geography, University of Colorado, Boulder, CO 80309.]
- , and G. J. McCabe, 1998: Verification of the Rhea-orographic-precipitation model. *J. Amer. Water. Res. Assoc.*, **34** (1), 103–112.
- Hill, F. F., K. A. Browning, and M. J. Bader, 1981: Radar and rain gauge observations of orographic rain over south Wales. *Quart. J. Roy. Meteor. Soc.*, **107**, 643–670.
- Isakson, A., 1996: Rainfall distribution over central and southern Israel induced by large-scale moisture flux. *J. Appl. Meteor.*, **35**, 1063–1075.
- Kalnay, E., and Coauthors, 1996: The NCEP/NCAR 40-Year Reanalysis Project. *Bull. Amer. Meteor. Soc.*, **77**, 437–471.
- Kuligowski, R. J., and A. P. Barros, 1998: Experiments in short-term precipitating forecasting using artificial neural networks. *Mon. Wea. Rev.*, **126**, 470–482.
- Olson, D. A., N. V. Junker, and B. Korty, 1995: Evaluation of 33 years of quantitative precipitation forecasting at the NMC. *Wea. Forecasting*, **10**, 498–511.
- Pandey, G. R., D. R. Cayan, M. D. Dettinger, and K. P. Georgakakos, 1998: Downscaling of precipitation distributions within the Sierra Nevada from global atmospheric fields. *Proc. 17th Conf. on Hydrology*, Dallas, TX, Amer. Meteor. Soc., 87–89.
- , —, and K. P. Georgakakos, 1999: Precipitation structure in the Sierra Nevada of California during winter. *J. Geophys. Res.*, **104**, 12 019–12 030.
- Rango, A. L., and P. V. Hobbs, 1994: Ice particle concentrations and precipitation development in small continental cumuliform clouds. *Quart. J. Roy. Meteor. Soc.*, **120**, 573–601.
- Rhea, J. O., 1978: Orographic precipitation model for hydrometeorological use. Atmospheric Paper 278, Colorado State University, Fort Collins, CO, 198 pp. [Available from Department of Atmospheric Sciences, Colorado State University, Fort Collins, CO 80523.]
- Robichaud, A. J., and G. L. Austin, 1988: On the modeling of warm orographic rain by the seeder–feeder effect. *Quart. J. Roy. Meteor. Soc.*, **114**, 967–988.
- Rogers, E., T. L. Black, D. G. Deaven, G. J. DiMego, Q. Zhao, M. Bladwin, N. W. Junker, and Y. Lin, 1996: Changes to operational early Eta analysis/forecast system at the National Centers for Environmental Prediction. *Wea. Forecasting*, **11**, 391–413.
- Sinclair, M. R., 1994: A diagnostic model for estimating orographic precipitation. *J. Appl. Meteor.*, **33**, 1163–1175.
- Speers, P., and C. F. Mass, 1986: Diagnosis and prediction of precipitation in regions of complex terrain. Washington State Dept. of Transportation Rep. WA-RD 91.1, 159 pp. [Available from Washington State Department of Transportation Library, P.O. Box 47425, 310 Maple Park Ave. S.E., Olympia, WA 98504.]
- Speers-Hayes, P., 1991: Prediction of precipitation in western Washington state. Washington State Dept. of Transportation Rep. WA-RD 231.1, 65 pp. [Available from Washington State Department of Transportation Library, P.O. Box 47425, 310 Maple Park Ave. S.E., Olympia, WA 98504.]
- Wallace, J. M., and P. V. Hobbs, 1977: *Atmospheric Science; An Introductory Survey*. Academic Press, 467 pp.